Improving Stability and Photoelectrochemical Performance of $BiVO_4$ Photoanodes in Basic Media by Adding a $ZnFe_2O_4$ Layer

Tae Woo Kim[1,2] and Kyoung-Shin Choi[1,*]

[1]Department of Chemistry, University of Wisconsin-Madison, Madison, WI 53706, USA.
[2]Energy Materials Laboratory, Korea Institute of Energy Research, 152 Gajeong-ro, Yuseong-gu, Daejeon 34129, Korea

Supporting Information

* Corresponding author. E-mail: kschoi@chem.wisc.edu

Experimental Section

Synthesis of $BiVO_4/ZnFe_2O_4$ electrodes. The nanoporous $BiVO_4$ electrode used in this study was prepared using the method reported in our recent paper.[1] A $ZnFe_2O_4$ layer was deposited on the surface of the $BiVO_4$ electrode by a two-step procedure; (1) photodeposition of FeOOH and (2) conversion of FeOOH to $ZnFe_2O_4$ (Scheme S1).

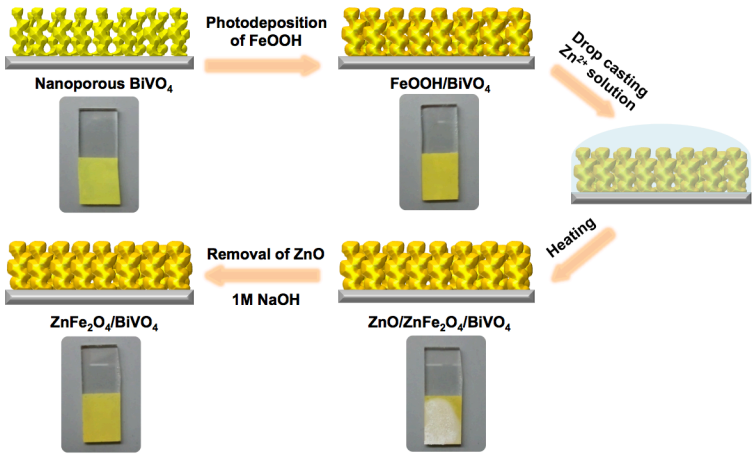

Scheme S1. Schematic representation of the synthesis procedure to form $BiVO_4/ZnFe_2O_4$ electrodes.

The photodeposition of FeOOH on the surface of the $BiVO_4$ electrode was first carried out in an undivided three-electrode cell consisting of a $BiVO_4$ working electrode (WE), a Pt counter electrode (CE), and a Ag/AgCl (4 M KCl) reference electrode (RE). A 300 W Xe arc lamp (Oriel Newport) with an AM 1.5G filter, neutral density filters and a water filter (IR filter) was used as the light source. The light was illuminated through the FTO contact (back-side illumination), and the light intensity at the FTO surface was adjusted to 1 mW/cm^2, which was measured using a research radiometer (International Light, IL 1700) coupled with a thermopile detector (International Light, SED623/H/N/K15). A 0.1 M $FeSO_4$ solution (pH 3.2-3.8) was used as the plating solution, and the solution was purged with nitrogen gas for 30 min prior to use. The solution was stirred gently during deposition. To facilitate photodeposition, an external bias of *ca.* 0.24-0.28 V vs. Ag/AgCl (4 M KCl), which was the open circuit potential of the $BiVO_4$ electrodes in the solution in the dark, was applied using a potentiostat (Bio Logic SP-200) during photodeposition. After photodeposition, electrodeposition of FeOOH was additionally carried out in the same solution by applying +1.2 V vs. Ag/AgCl (4 M KCl) for 1 min. This was to deposit FeOOH

on any bare $BiVO_4$ or FTO surfaces exposed to the electrolyte. After deposition, $BiVO_4$/FeOOH electrodes were washed with deionized water and dried at room temperature.

The thickness of the FeOOH layer was varied by changing the deposition time (10-60 min), and the optimum thickness of the FeOOH layer was determined by examining the photocurrent and stability of the resulting $BiVO_4/ZnFe_2O_4$ electrodes. The results show that $BiVO_4/ZnFe_2O_4$ electrodes prepared from depositing FeOOH for approximately 40 min (equivalent to passing a total charge of 65-70 mC/cm^2) achieve the best performance in terms of both photocurrent and stability (Figures S4).

The conversion of FeOOH to $ZnFe_2O_4$ was achieved by annealing the electrodes in a muffle furnace at 550 ^oC for 1 h in air (ramping rate = 2 °C/min) after drop casting 0.05 mL-0.1 mL of 0.5 M $Zn(NO_3)_2 \cdot 6H_2O$ on the $BiVO_4$/FeOOH electrodes. The lateral dimension of the $BiVO_4$/FeOOH film was 1 cm x 1.3 cm, and the thickness of the $BiVO_4$/FeOOH film was ~750 ± 40 nm. Following the heat-treatment, excess ZnO present on the $BiVO_4/ZnFe_2O_4$ films was removed by soaking the $BiVO_4/ZnFe_2O_4$/ZnO films in 1 M NaOH solution for 30-60 minutes at 30-35 ^oC. Finally, the resulting $BiVO_4/ZnFe_2O_4$ electrodes were thoroughly rinsed with DI water and dried at RT.

Co^{2+} adsorption on the surface of $BiVO_4/ZnFe_2O_4$. The $BiVO_4/ZnFe_2O_4$ electrodes were immersed in a 0.5 M cobalt nitrate ($Co(NO_3)_2 \cdot 6H_2O$) solution for 5 minutes followed by rinsing with DI water. The amount of Co^{2+} adsorbed could be adjusted by repeating this process. Typically, we obtained optimized PEC performance after about two or three cycles of Co^{2+} adsorption.

Characterization. The purity and crystal structure of the $BiVO_4/ZnFe_2O_4$ electrodes were examined by powder X-ray diffraction (Bruker D8 Advanced PXRD, λ = 1.5418 Å, 298 K, Ni-filtered Cu K_α-radiation). The surface morphology and chemical composition of the $BiVO_4/ZnFe_2O_4$ electrodes were probed by scanning electron microscopy (SEM, a LEO 1530, an accelerating voltage of 5 kV). The chemical composition of the $BiVO_4$ electrode was confirmed to be 0.97 ± 0.02 for Bi/V, and the chemical composition of the $ZnFe_2O_4$ layer was confirmed to be 0.51 ± 0.02 for Zn/Fe by a Hitachi S3400-N scanning electron microscope equipped with an energy dispersive X-ray spectrometer (EDS) (Thermo Fisher Scientific Inc.). The uniformity and crystallinity of FeOOH or $ZnFe_2O_4$ layers deposited on $BiVO_4$, which were too thin to be examined by other methods, were confirmed by high resolution-

transmittance electron microscopy (HRTEM) and selected area electron diffraction (SAED) using a JEOL JEM-2100F microscope at an accelerating voltage of 200 kV. X-ray photoelectron spectroscopy (XPS) spectra of Zn and Fe in the $BiVO_4/ZnFe_2O_4$ were recorded using a K-Alpha X-ray photoelectron spectrometer (Thermo Scientific Inc.) equipped with a monochromated Al Kα line as the X-ray source. The binding energies were calibrated with respect to the residual C 1s peak at 284.6 eV. UV-vis absorption spectra were obtained on a Cary 5000 UV-vis spectrophotometer (Agilent), in which the sample was fixed in the center of an integrating sphere to measure all light reflected and transmitted to accurately assess the absorbance. A FTO substrate was used as the reference for these absorption measurements.

Photoelectrochemical measurements. PEC characteristics of photoelectrodes prepared in this work were evaluated in the same system described in photodeposition of FeOOH above. Illumination through the FTO side (back-side illumination) was used. The power intensity of the incident light was calibrated to 100 mW/cm^2 at the surface of the FTO substrate (before the light penetrates FTO) by using a research radiometer (International Light, IL 1700) coupled with a thermopile detector (International Light, SED623/H/N/K15) and a NREL certified reference cell (Photo Emission Tech., Inc.). The beam passed through an optical fiber, and the active area of the sample exposed to electrolyte was 0.1-0.2 cm^2. Photocurrent measurements were performed in 0.1 M potassium hydroxide (KOH, pH 13). Prior to measurements, the electrolyte was thoroughly deaerated by purging it with nitrogen for 30-60 min. Photocurrents were monitored either while sweeping the potential to the anodic direction with a scan rate of 10 mV/s or while applying a constant bias. While all measurements were carried out using a Ag/AgCl (4M KCl) reference electrode, all results in this work were shown against the reversible hydrogen electrode (RHE) for ease of comparison with H_2 and O_2 redox levels and other reports that used electrolytes with different pH conditions. The conversion between potentials vs. Ag/AgCl and vs. RHE is determined using the equation below.

$$E\ (\text{vs. RHE}) = E\ (\text{vs. Ag/AgCl}) + E_{Ag/AgCl}\ (\text{reference}) + 0.0591\ \text{V} \times \text{pH}$$

$$(E_{Ag/AgCl}\ (\text{reference}) = 0.1976\ \text{V vs. NHE at 25 ºC})$$

Incident photon-to-current efficiency (IPCE) at each wavelength was determined using illumination from a 300 W Xe arc lamp (Oriel Newport) passed through an AM 1.5G

filter, neutral density filters, and a water filter to approximate the output of the sun. Monochromatic light was produced using an Oriel Cornerstone 130 monochromator with a 10-nm bandpass. The intensity of incident light was measured using a research radiometer (International Light, IL 1700) with a calibrated silicon photodiode detector (International Light, SED033). IPCE was measured in 0.1 M KOH (pH 13) with the same three-electrode setup described above for photocurrent measurements, using a Princeton Applied Research Potentiostat/Galvanostat model 263A to apply 1.23 V vs. RHE. Absorbed photon-to-current efficiency (APCE) was obtained by dividing the IPCE by the light harvesting efficiency (LHE) at each wavelength using the following equations.

$$\text{APCE}\ (\%) = \text{IPCE}\ (\%) \ / \ \text{LHE}$$

$$\text{LHE} = 1 - 10^{-A_{(\lambda)}} \quad (A_{(\lambda)}\text{: absorbance at wavelength } \lambda)$$

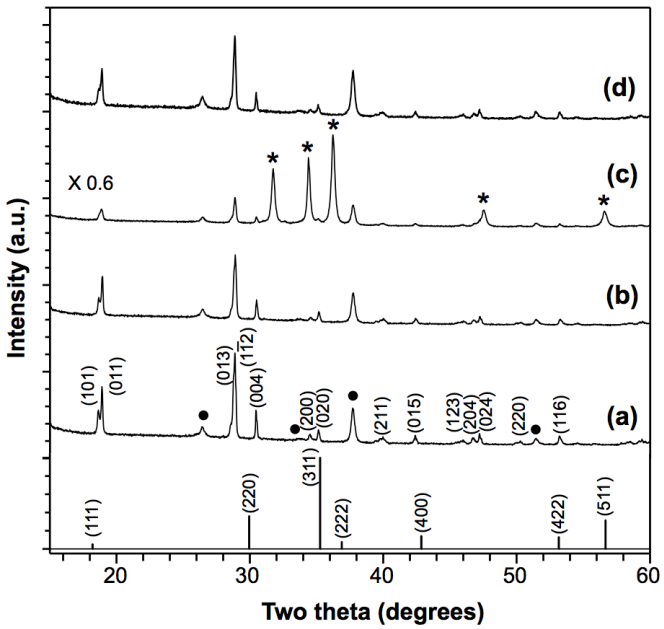

Figure S1. XRD patterns of (a) pristine $BiVO_4$, (b) $BiVO_4$/FeOOH, (c) $BiVO_4/ZnFe_2O_4$ with excess ZnO, and (d) $BiVO_4/ZnFe_2O_4$ after ZnO removal. The (hkl) indices of $BiVO_4$ in (a) are based on JCPDF 83-1699 (Space group: I 2/b). Circles in (a) and asterisks in (c) represent peaks from FTO substrate and crystalline ZnO, respectively. Vertical bars at the bottom of the figure represent expected positions and relative intensities of diffraction peaks by $ZnFe_2O_4$ (JCPDS No. 77-0011). The fact that the patterns shown in (a) and (d) are identical suggests that the $ZnFe_2O_4$ layer is X-ray amorphous. However, the nanocrystallinity and the phase of the $ZnFe_2O_4$ layer were confirmed by the selected area electron diffraction shown in Figure 1(f) in the main text.

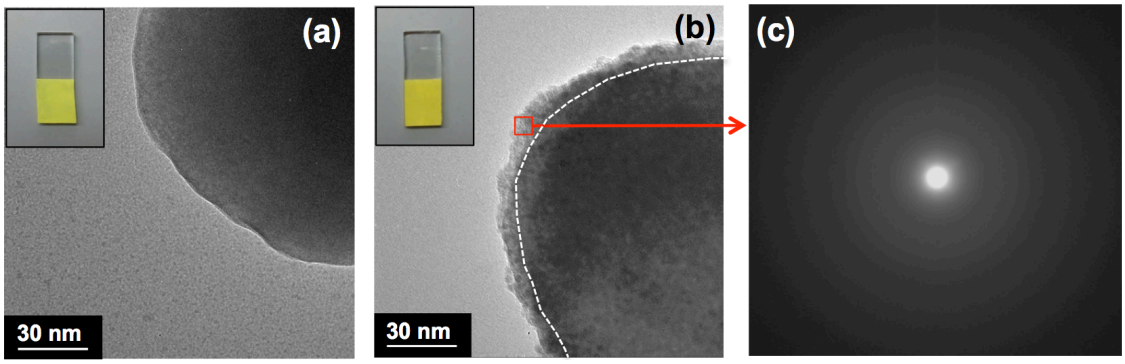

Figure S2. TEM images of (a) pristine $BiVO_4$ and (b) $BiVO_4$/FeOOH; (c) SAED pattern of a rectangular area in (b) showing the amorphous nature of the FeOOH layer. The insets of (a) and (b) show the photographs of the $BiVO_4$ and $BiVO_4$/FeOOH electrodes.

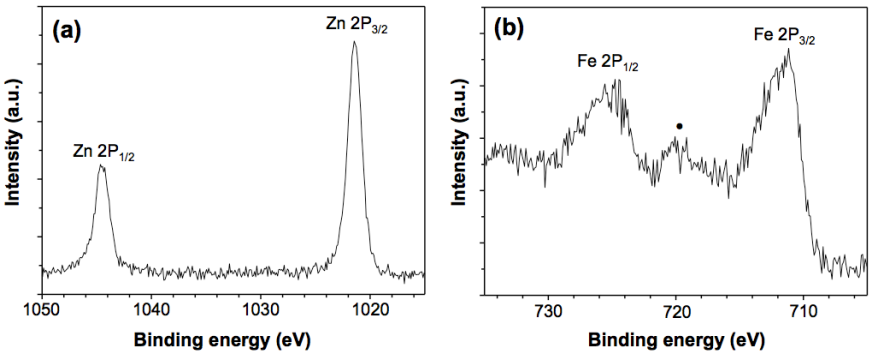

Figure S3. XPS spectra of (a) Zn 2p and (b) Fe 2p peaks of $BiVO_4/ZnFe_2O_4$. In (b), a dot shown around 719 eV indicates a satellite peak of Fe^{3+} $2p_{3/2}$. The Zn $2p_{3/2}$ and Zn $2p_{1/2}$ peaks shown in (a) are centered at 1022.8 eV and 1044.4 eV, respectively, which are consistent with the values reported for $ZnFe_2O_4$ with the oxidation state of Zn^{2+}.[2-4] In the case of the Fe XPS spectrum shown in (b), the Fe $2p_{3/2}$ peak centered at 710.6 eV and the Fe $2p_{1/2}$ peak centered at 724.4 eV as well as a satellite peak of the Fe 2p appearing at 719.5 eV confirm the oxidation state of Fe^{3+} ions in the $ZnFe_2O_4$ layer.[2-4]

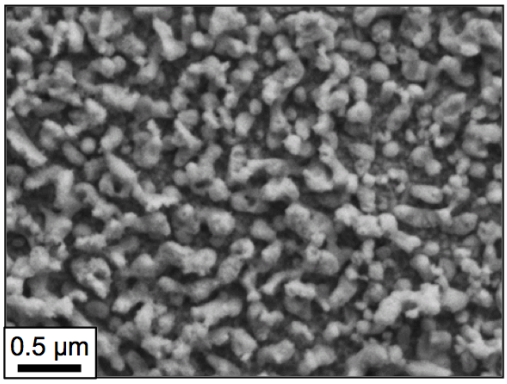

Figure S4. SEM image of a $BiVO_4/ZnFe_2O_4/Co^{2+}$ electrode after J-t measurement showing photoanodic disssolution of $BiVO_4$.

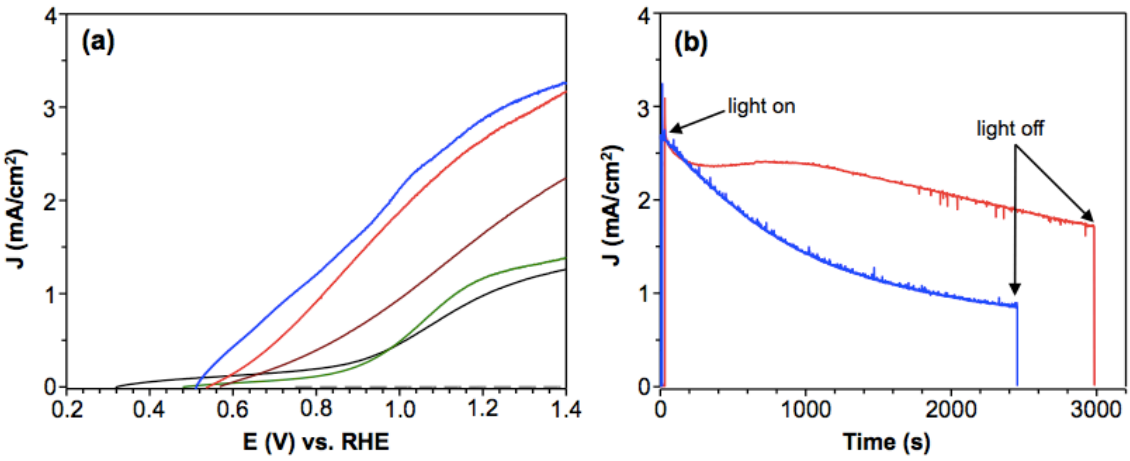

Figure S5. (a) J-V plots obtained in 0.1 M KOH (pH 13) under AM 1.5G, 100 mW/cm^2 illumination; $BiVO_4$ (black), $BiVO_4/ZnFe_2O_4$-10 min (green), $BiVO_4/ZnFe_2O_4$-20 min (blue), $BiVO_4/ZnFe_2O_4$-40 min (red), and $BiVO_4/ZnFe_2O_4$-60 min (brown). The dark current was indicated as gray-dashed lines. (b) J-t plots meausred at 1.23 V vs. RHE in the same solution. The color codes used in (b) are the same as those used in (a). The Fermi level of $BiVO_4$ is not expected to be altered by the addition of a thin $ZnFe_2O_4$ layer, which has a Fermi level that should be comparable to that of $BiVO_4$. However, the point of zero zeta potential of $ZnFe_2O_4$ (7.3–9.3) is reported to be much higher than that of $BiVO_4$ (2.5–3.5).[1,5-8] Since the Helmholtz layer potential drop of the $BiVO_4/ZnFe_2O_4$ electrode at the solid/solution interface should be governed by the outermost $ZnFe_2O_4$ layer, the flatband potential of the $BiVO_4/ZnFe_2O_4$ electrode should be more positive than that of $BiVO_4$. This is why the photocurrent onset of the $BiVO_4/ZnFe_2O_4$ electrode is shifted to the positive direction when a thin layer of $ZnFe_2O_4$ is added on the surface of $BiVO_4$. As the thickness of the $ZnFe_2O_4$ layer increases, photon absorption, electron-hole separation, and charge transport of the $BiVO_4/ZnFe_2O_4$ electrode is affected more by the presence of the $ZnFe_2O_4$ layer. The $BiVO_4/ZnFe_2O_4$-40 min electrode appears to possess an optimum thickness of the $ZnFe_2O_4$ layer considering all the effects as well as the stability.

References

(1) Kim, T. W.; Choi, K. -S. Nanoporous $BiVO_4$ Photoanodes with Dual-layer Oxygen Evolution Catalysts for Solar Water Splitting. *Science* **2014**, *343*, 990−994.

(2) Dom, R.; Subasri, R.; Hebalkar, N. Y.; Chary, A. S.; Borse, P. H. Synthesis of a Hydrogen Producing Nanocrystalline $ZnFe_2O_4$ Visible Light Photocatalyst Using a Rapid Microwave Irradiation Method. *RSC Adv.* **2012**, *2*, 12782−12791.

(3) Song, H.; Zhu, L.; Li, Y.; Lou, Z.; Xiao, M.; Ye, Z. Preparation of $ZnFe_2O_4$ Nanostructures and Highly Efficient Visible-Light-Driven Hydrogen Generation with the Assistance of Nanoheterostructures. *J. Mater. Chem. A* **2015**, *3*, 8353−8360.

(4) Lian, L.; Hou, L.; Zhou, L.; Wang, L.; Yuan, C. Rapid Low-Temperature Synthesis of Mesoporous Nanophase $ZnFe_2O_4$ with Enhanced Lithium Storage Properties for Li-ion Batteries. *RSC Adv*. **2014**, *4*, 49212−49218.

(5) Castillo, N. C.; Heel, A.; Graule, T.; Pulgarin, C. Flame-assisted Synthesis of Nanoscale, Amorphous and Crystalline, Spherical $BiVO_4$ with Visible-light Photocatalytic Activity. *Appl. Catal. B* **2010**, *95*, 335−347.

(6) S. Obregón, G. Colón, On the different photocatalytic performance of $BiVO_4$ catalysts for Methylene Blue and Rhodamine B degradations. *J. Mol. Catal. A: Chem*. **2013**, *376*, 40−47.

(7) Iqubal, M. A.; Sharma, R.; Kamaluddin Studies on Interaction of Ribonucleotides with Zinc Ferrite Nanoparticles Using Spectroscopic and Microscopic Techniques. *Karbala Int. J. Mod. Sci.* **2015**, *1*, 49-59.

(8) Rekhila, G.; Trari, M.; Bessekhouad, Y. Characterization and Application of the Hetero-junction ZnFe2O4/TiO2 for Cr(VI) Reduction under Visible Light. *Appl. Water Sci.* **2015**, DOI 10.1007/s13201-015-0340-9.